Free energy of adhesion of lipid bilayers on silica surfaces

M. Schneemilch, and N. Quirke

Citation: The Journal of Chemical Physics **148**, 194704 (2018); doi: 10.1063/1.5028557
View online: https://doi.org/10.1063/1.5028557
View Table of Contents: http://aip.scitation.org/toc/jcp/148/19
Published by the American Institute of Physics

Free energy of adhesion of lipid bilayers on silica surfaces

M. Schneemilch and N. Quirke[a)]
Department of Chemistry, Imperial College London, London SW7 2AY, United Kingdom

(Received 12 March 2018; accepted 1 May 2018; published online 21 May 2018)

The free energy of adhesion per unit area (hereafter referred to as the adhesion strength) of lipid arrays on surfaces is a key parameter that determines the nature of the interaction between materials and biological systems. Here we report classical molecular simulations of water and 1,2-dimyristoyl-sn-glycero-3-phosphocholine (DMPC) lipid bilayers at model silica surfaces with a range of silanol densities and structures. We employ a novel technique that enables us to estimate the adhesion strength of supported lipid bilayers *in the presence of water*. We find that silanols on the silica surface form hydrogen bonds with water molecules and that the water immersion enthalpy for all surfaces varies linearly with the surface density of these hydrogen bonds. The adhesion strength of lipid bilayers is a linear function of the surface density of hydrogen bonds formed between silanols and the lipid molecules on crystalline surfaces. Approximately 20% of isolated silanols form such bonds but more than 99% of mutually interacting geminal silanols do not engage in hydrogen bonding with water. On amorphous silica, the bilayer displays much stronger adhesion than expected from the crystalline surface data. We discuss the implications of these results for nanoparticle toxicity. https://doi.org/10.1063/1.5028557

I. INTRODUCTION

The interaction of cell membranes with inorganic surfaces is of interest in medicine and in toxicology. In medicine, inorganic materials are used in implants and in finely divided form (nanoparticles) as nanomedicines or magnetic resonance imaging (MRI) contrast agents.[1–4] Inorganic engineered nanoparticles (ENMs) are increasingly found in the environment. They are present in batteries, catalysts, chemical coatings, packaging, electronic devices, and cosmetics.[5] The expanding production of ENMs has led to serious concerns regarding their impact on human health and the environment in general.[5] Most recently the focus of research has been on the interaction of nanoparticles with cytoplasmic membranes with a view to assessing likely damage due to nanoparticles at the cellular level.[6] At the same time, there is interest in experiments on model membranes comprising lipid vesicles with the goal of understanding the factors that control particle uptake in these much simpler systems.[7,8]

According to the Helfrich membrane model[9] applied by Deserno *et al.*[10,11] to the wrapping of spherical particles by membranes, the fate of the particle is determined by whether the adhesion strength is sufficient to overcome the bending energy associated with membrane deformation during particle wrapping. Particles smaller than a critical size, determined by the balance of these opposing drivers, will not adhere to the membrane. Larger particles will adhere and will undergo wrapping, the extent of which is determined by the membrane tension. With low tension and/or strong adhesion, particles will undergo complete engulfment, following which the particle detaches from the membrane leaving a membrane pore through which cytosol leakage can occur. Since it is the driving force for the process, any comprehensive assessment of the potential nanotoxicity of a material must include an estimate of the membrane adhesion strength.

Such data will be helpful in developing models of *passive* nanoparticle uptake by human cells and of pulmonary surfactant disruption due to the presence of nanoparticles in the alveolar spaces. The classic example of passive nanoparticle uptake occurs during the interaction of particles with red blood cells, which lack the cellular machinery to sequester foreign particles. Haemolysis, as the uptake process is termed, can be readily detected by the presence of the leaked cytosol. Furthermore, the mechanism appears to be related to other negative outcomes; Warheit *et al.*[12] showed that the inflammation response to nanoparticles after inhalation is correlated with their haemolytic potential. Adhesion strength data may also prove useful in understanding certain other aspects of activated uptake processes, such as macrophage overload.[13]

Silica nanoparticles are widely used in many industrial and biomedical applications and are generally considered to be biocompatible and of low cytotoxicity. However, under certain conditions, they are known to induce haemolysis in red blood cells. Inhalation of silica nanoparticles can be hazardous, inducing an inflammation response and in severe cases silicosis.[19,20] Unfortunately, there are relatively few experimental data for the adhesion strength that would allow us to better understand these toxicity pathways.[14] The only direct measurement of the adhesion strength of lipid bilayers on silica surfaces, as far as we aware, was performed by Anderson *et al.*[15] using a surface force apparatus. 1,2-dimyristoyl-sn-glycero-3-phosphocholine (DMPC) supported lipid bilayers

[a)]Author to whom correspondence should be addressed: n.quirke@ic.ac.uk

(SLBs), formed by fusion of vesicles or Langmuir-Blodgett deposition, were contacted by electron-deposited amorphous silica surfaces in phosphate-buffered saline solution. The adhesion strength was −0.5 mN m^{-1} with vesicle fusion bilayers and −1 mN m^{-1} with Langmuir-Blodgett deposition.

Applying the greater of these two values in combination with a typical bilayer bending modulus[16] of 10^{-19} J, elastic theory predicts that the critical diameter for spherical silica particles is approximately 27 nm. However, this value appears rather large compared to other observations of particle-bilayer interactions from which estimates of the critical size can be deduced. For example, Roiter *et al.*[8] deposited a bilayer on silica particles positioned on a mica surface and found that the bilayer followed the contours of particles as small as 22 nm in diameter. Strobl *et al.*[17] directly observed the uptake of 22 nm particles by giant unilamellar DMPC vesicles using confocal microscopy. The critical diameter of 22 nm suggested by these experiments implies that the adhesion strength was around −1.5 mN m^{-1}. Furthermore, Pera *et al.*[18] found that silica particles as small as 16 nm in diameter could induce leakage from 1,2-dioleoyl-sn-glycero-3-phosphocholine (DOPC) vesicles, indicating that the adhesion strength can be as great as −2.7 mN m^{-1}.

These studies suggest that adhesion strength can vary markedly depending on a variety of factors including the particle shape and structure as well as the pH and ion concentration of the surrounding medium. For example, the work of Pavan *et al.*[19,20] with silica particles points to specific distributions of silanols/siloxanes on the silica surface having a major role in determining the extent of the inflammation response to inhaled particles. It is clear that a detailed understanding of the link between surface structure and adhesion strength is required in the assessment of potential toxicity and the design of safe nanoparticles. Unfortunately, many of the experiments discussed here have little detailed surface characterisation which might have shed light on this link.

Where experimental data are lacking, molecular simulation of well-calibrated molecular models provides an alternative route to physical property data. This approach offers advantages; the atomistic structure of the surface can be completely specified and key features can be varied systematically. In a previous paper, we introduced a method for determining the adhesion strength of lipid bilayers on surfaces in the presence of water from molecular simulation[21] and demonstrated its application with a study of DMPC bilayer adhesion to a model gold surface. Here, we apply the method to DMPC-silica systems using fully atomistic models that have been shown to reproduce many crucial physical properties. The surfaces were characterised by estimating physical properties central to the adhesion process such as the silanol density and the solvent accessible surface area. Additionally, we estimated the heat of immersion for each of the surfaces, as previous work on this subject has indicated that the strength of bilayer adhesion is influenced by the strength of adhesion of the water in the contact layer, at least part of which must be displaced for bilayer adhesion to occur. Finally, we measured the free energy of adsorption of isolated lipid molecules on the surfaces.

II. METHODOLOGY

The DMPC lipids were modelled using the fully atomistic 118 site Slipids force field which was developed for use in conjunction with TIP3P water.[22–24] This system was shown to reproduce many experimentally observed properties of bilayers such as the lipid specific area and volume, bilayer thickness, isothermal area compressibility, and nuclear magnetic resonance (NMR) order parameters and scattering form factors. The silica force field and initial configurations of the silica surfaces employed in this study were published by Emami *et al.*[25] They have shown the model to accurately predict bulk properties of α-quartz and α-cristobalite as well as certain properties of the interface with water such as the immersion enthalpy, contact angle and adsorption isotherm. The same force field has been recently utilised for studies of bilayer adhesion[26] and single molecule adsorption studies.[27,28] Although the force field includes interaction potentials for ionised silanol sites, in this study we employ only fully hydroxylated surfaces, which are exhibited in non-ionic solution or at the point of zero charge (approximately pH 2) in the presence of ions. The interaction potentials between DMPC and silica sites were generated using Lorentz-Berthelot mixing rules.

We employed a representative subset of the surfaces in the published database which are here identified by the coordination number of the surface silicon atoms. Accordingly, the Q^2 surface was composed of 2-fold coordinated silicon atoms, which were derived from the (100) cleavage plane of α-quartz and had a silanol surface density of 9.4 nm^{-2}. The crystalline Q^3 surface was derived from the $(10\bar{1})$ cleavage plane of α-cristobalite. The Q^4 surface corresponds to a heat treated Q^3 surface with all silanol groups condensed to form siloxane bridges. In addition, we employed an amorphous surface (denoted Q^{3a}) provided in the published database, which was based on the Q^3 surface and is typical of precipitated nanoparticles.[29] The surfaces were characterised by estimates of the solvent accessible area, calculated using a solvent molecule 0.14 nm in diameter. These values, expressed as a ratio of the projected surface area, are recorded in Table I.

All simulations were performed using GROMACS 5.1.2 software with a 2 fs time step. Temperatures were maintained at 310 K using the Nose-Hoover thermostat with 5 ps time constant. Pressure was maintained at 1 atm using an anisotropic Parrinello-Rahman barostat with 10 ps time constant. Electrostatics were calculated with a Particle Mesh Ewald (PME) summation. Although during calibration of the DMPC model Lennard-Jones and real space electrostatic interaction potentials were truncated at 1.5 nm, we employed a 1.2 nm cutoff identical to that used in the silica force field. Error estimates were obtained by block averaging unless stated otherwise.

A. Heat of immersion

The change in enthalpy upon immersion was estimated by conducting simulations of three systems: the surface in contact with water, the surface in a vacuum, and a simulation of bulk water containing an identical number of water molecules as

TABLE I. Properties of the silica-water interfaces.

Surface	Q^2	Q^3	Q^{3a}	Q^4
Silanol density (nm^{-2})	9.55	4.86	5.02	0
Solvent accessible area ratio	1.16	1.3	1.39	1.14
Silica-water hydrogen bond density (nm^{-2})	5.7 ± 0.3	8.3 ± 0.3	6.5 ± 0.3	1.2 ± 0.2
Heat of immersion ($mN\ m^{-1}$)	76.7 ± 0.8	151.2 ± 1.3	117.2 ± 1.9	−22.2 ± 0.8
Adsorption energy ($kJ\ mol^{-1}$)	−2.5	−15.8	−3.8	−53.6
Adsorption enthalpy ($kJ\ mol^{-1}$)	9.1 ± 8.3	−21 ± 6.9	−69.2 ± 10.8	−64.8 ± 9.1

the first system. The immersion enthalpy, ΔH_{imm}, was then calculated using the following equation:

$$\Delta H_{imm} = \frac{1}{2A}\left(H_{surface-water} - H_{surface-vacuum} - H_{water}\right), \quad (1)$$

where H is the enthalpy of the system and A is the area of the interface. All systems were simulated for 400 ns with 10 ns equilibration.

B. Adhesion strength

Surface slabs were constructed with surface dimensions of approximately 30 × 4 nm, as shown in Fig. 1. Equilibrated bilayer ribbons were then brought into contact with the silica surfaces. In contrast to the gold model studied previously,[21] bilayer patches on silica surfaces are stable. Therefore, it was sufficient to constrain only one end of the ribbon at a distance of 10 nm from the centre of the slab, as depicted in Fig. 1. A total of 18 lipids comprised the pull group at the edge of the ribbon. The distribution of lipids in the ribbon was maintained at equilibrium by periodically updating the lipids in the pull group as described in our previous paper.[21] The constraint force, F, required to keep the end of the ribbon at a distance h above the surface was monitored during the simulation. The constraint force is related to the adhesion strength k_w by

$$k_w = F\frac{dh}{dA}, \quad (2)$$

where dA is the increase in the area of the adsorbed bilayer resulting from a reduction in the restraint of height by dh.

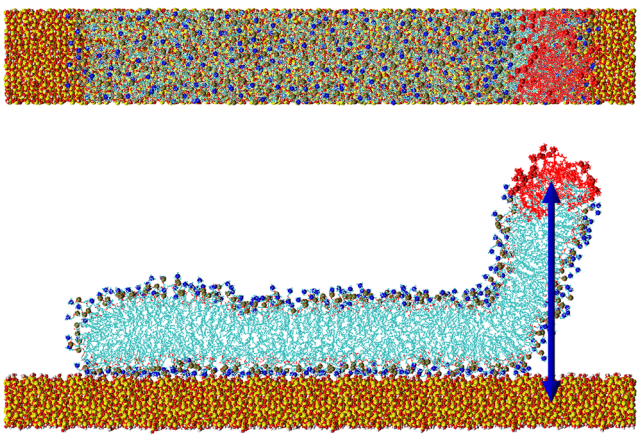

FIG. 1. Snapshot of a lipid ribbon adsorbed on the amorphous Q^3 (Q^{3a}) surface. Water is omitted for clarity. The lipids in red constitute the pull group which is restrained by a harmonic potential depicted by the blue arrow.

The ratio dh/dA is the product of twice the inverse of the area per lipid in the supported lipid bilayer and the inverse of dn/dh, where n is the number of lipids in the free section of the bilayer. The ratio dn/dh is estimated from the one-dimensional lipid number density profile perpendicular to the surface at the point where the magnitude of the gradient is at the minimum. Note that the adhesion strength can be expected to be independent of the restraint height as long as the length of the ribbon is sufficient to ensure that at least some portion of the adhering ribbon is representative of the "bulk" adhesion density, i.e., is not affected by proximity to the edges.

C. Single lipid adsorption free energy

A single DMPC molecule was inserted into the water channel formed between periodic images of a silica surface unit. The water channel was approximately 12 nm wide. A harmonic potential was applied between the centres of mass of the silica slab and the DMPC molecule in each of 40 umbrella windows. The grid spacing of umbrella windows was 0.1 nm and the force constant was 1000 $kJ\ mol^{-1}\ nm^{-2}$. After 15 ns of equilibration, data were collected in each window over 50 ns production runs. The potential of mean force was calculated using the weighted histogram analysis method.[30]

III. RESULTS

A. Silica-water interface

The silica-water interface was characterised by estimation of the heat of immersion in water, the results of which are recorded in Table I. The heat of immersion was found to be endothermic on the relatively hydrophobic Q^4 surface and increasingly exothermic on the Q^2, Q^{3a}, and Q^3 surfaces; ranging from $-22.2 \pm 0.8\ mN\ m^{-1}$ to $151.2 \pm 1.3\ mN\ m^{-1}$. It has been proposed[31] that the heat of immersion is primarily dictated by two interactions: hydrogen bonds between water and silanol groups and interactions between permanent dipole moments of water and the polarity of the surface. Hydrogen bonds in the simulation trajectory were identified using the GROMACS analysis tool gmx hbond and the time averaged surface density recorded in Table I. Additional detail on the distribution of charge and hydrogen bonding along the surface normal is provided in the supplementary material.

The heat of immersion did not simply correlate with the silanol surface density. The Q^2 surface, with the greatest

surface density of silanols at 9.55 nm^{-2}, had the lowest heat of immersion of the silanol bearing surfaces (76.7 ± 0.8 mN m^{-1}), whilst the Q^3 surface, with a silanol density of only 4.86 nm^{-2}, displayed the greatest heat of immersion. There is, however, a strong, approximately linear, correlation between the total silica-water hydrogen bond density and the heat of immersion, with each additional hydrogen bond contributing approximately 15 kJ mol^{-1} to the heat of immersion. This is in qualitative agreement with *ab initio* simulations of the binding energy of water molecules with isolated silanol groups by Saengsawang *et al.*[32] In their study, they identified three main types of hydrogen bonds between silanol and water; in the first a silanol donates the hydrogen to a single hydrogen bond, in the second the silanol accepts a hydrogen from the water molecule, and in the third a silanol interacts with two water molecules acting as both a donor and acceptor. The binding energies of each type were approximately −30, −19, and −52 kJ mol^{-1}.

Evidently, the geminal silanols on the Q^2 surface are far less effective in forming hydrogen bonds with water than the isolated silanols on the Q^3 surface; roughly 56% of the geminal silanols on the Q^2 surface were involved in at least one hydrogen bond on average, whereas this figure was 96% for the isolated silanols on the crystalline Q^3 surface. On the amorphous Q^{3a} surface, 80% of the silanols were involved in at least one hydrogen bond with water. Examination of the hydrogen bonding between adjacent surface silanols—referred to as mutually interacting silanols—shows that on the Q^2 surface 94% of the silanols were involved in at least one mutual interaction (either as a donor or acceptor). We also found that on the Q^3 surface, the time averaged fraction of silanols involved in at least one mutual interaction was less than 4%, while on the Q^{3a} surface the fraction was 37%. Clearly these results do not imply that silanols involved in a mutual interaction are completely precluded from forming hydrogen bonds with water. In fact, on the Q^2 surface, 54% of the silanols involved in a mutual interaction were also involved in a hydrogen bond with water. This value was even greater on the Q^3 surface, although the incidence of mutual interactions was very low. On the Q^{3a} surface, only 30% of the mutually interacting silanols formed hydrogen bonds with water. However, in comparison, the fraction of available silanols (not involved in mutual interactions) that were involved in a water hydrogen bond was 86%, 83%, and 62% on the Q^2, Q^3, and Q^{3a} surfaces, respectively. So while mutually interacting silanols were not entirely precluded from hydrogen bonding with water, they were less likely to do so.

Of the total number of silanols on the Q^3 surface, roughly 22% acted as donors in a single hydrogen bond, 10% as acceptors in a single hydrogen bond, and 64% acted as both a donor and acceptor in two hydrogen bonds, in qualitative agreement with the proportions suggested by the relative binding energies on isolated silanols reported by Saengsawang. On the Q^{3a} surface with a slightly greater silanol density, the fractions were 30%, 18%, and 32%, while on the Q^2 surface the fractions were 26%, 29%, and 2%. This declining incidence of silanols being involved in two hydrogen bonds on these surfaces is probably related to the increasing incidence of mutual interactions.

B. Single lipid adsorption

Here we examine the interaction of a single lipid with each surface, in order to glean more insight into bilayer adhesion. The potentials of mean force (PMF) for single lipid adsorption are plotted in Fig. 2. The adsorption (free) energies, corresponding to the minimum in the PMF, are recorded in Table I along with the adsorption enthalpies, which were estimated by the difference in total energy between simulations in which the lipid was adsorbed on the surface and in which the lipid was in the middle of the channel. The strongest adsorption energy, −53.6 kJ mol^{-1}, was recorded on the Q^4 surface. Also significant was the adsorption on the Q^{3a} surface which was estimated to be −15.8 kJ mol^{-1}. The Q^2 and Q^3 surfaces only weakly adsorb, with free energy magnitudes less than 4 kJ mol^{-1}. Snapshots of the lowest energy configurations are also shown. Both lipid tails adsorb flat to the Q^4 surface, with only the head group displaced from the surface. On the Q^{3a} surface, the head group is flat against the surface while only minimal contact is made with the lipid on the Q^2 and Q^3 surfaces.

It can be seen from the radial distribution functions (RDFs) included in the supplementary material that the lipid carbon tails preferentially adsorb on the Q^4 surface, along with the tail oxygen sites, while the lipid head group sites remain more distant. This suggests that the strong adsorption on this surface is driven by hydrophobic interactions between tail group atoms and the bridging oxygens on the surface. On the Q^{3a} surface, phosphorous-bonded oxygen atoms made the closest approach to both bridging and silanol oxygen sites. There is a particularly large peak for phosphorous-bonded oxygen in the silanol oxygen RDF, which is consistent with the idea that the rougher surface allows the lipid better access to the silanol sites. On the Q^2 and Q^3 surfaces, the snapshots show that the lipid adopts configurations that minimise the contact between the lipid and the surface. Note that while for the rest of the surfaces the entropic contribution to the adsorption energy opposes adsorption, on the Q^2 surface it appears to drive the adsorption process. We will address the source of the entropy increase in Sec. III C.

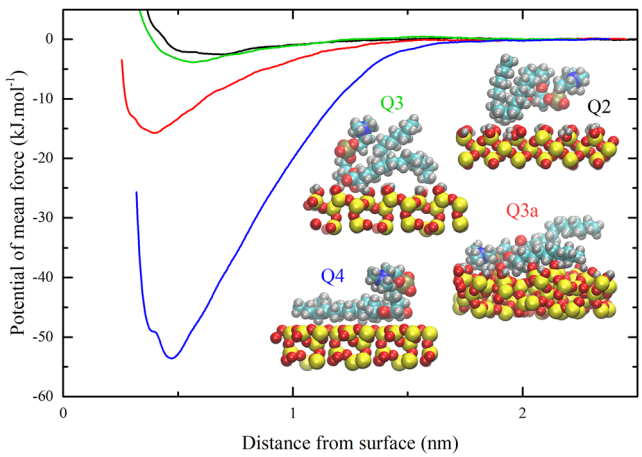

FIG. 2. The adsorption free energy of a single DMPC molecule in aqueous solution on each silica surface.

TABLE II. Properties of the silica-bilayer interfaces.

Surface	Q^2	Q^3	Q^{3a}	Q^4
a (nm^{-2})	0.65	0.67	0.71	0.64
Separation (nm)	0.76	0.54	0.52	1.01
Thickness (nm)	3.15	3.08	2.98	3.18
dh/dA (nm^{-1})	0.25	0.23	0.21	0.19
Adhesion strength (mN m^{-1})	−0.8 ± 0.3	−1.2 ± 0.3	−2.7 ± 0.5	−0.7 ± 0.2
Adhesion enthalpy (mN m^{-1})	2.1 ± 1.2	−2.8 ± 1.7	−10 ± 1.1	−3.4 ± 2.1
Silica-water hydrogen bond density (nm^{-2})	4.98	6.14	4.64	1.13
Silica-lipid hydrogen bond density (nm^{-2})	0.19	1.93	0.81	0

C. Silica-bilayer interface

The main object of this study is the adhesion strength (Table II), which is negative for all the surfaces indicating that DMPC bilayers will spontaneously adhere to silica. The Q^2 and Q^4 surfaces, despite being structurally distinct, display similar adhesion strengths: −0.77 ± 0.26 and −0.71 ± 0.18 mN m^{-1}, respectively. Adhesion on the Q^3 surface is stronger at −1.14 ± 0.26 mN m^{-1}. The Q^{3a} surface, on the other hand, has a much greater adhesion strength of −2.72 ± 0.52 mN m^{-1} despite having an identical composition to the Q^3 surface.

The key properties of the adsorbed bilayers, measured through the central region of the adsorbed section of the bilayer, are recorded in Table II. This region, typically several nm wide, was far enough from the edge of the bilayer to be representative of the "bulk" supported lipid bilayer (SLB), based on observation of bilayer properties (density and ApL) measured as a function of the distance normal to the ribbon edge. The time averaged projected ApL in the SLB represent moderate increases over the published values[22] for the free bilayer (~0.62 nm^2), ranging from 0.64 on the Q^4 surface to 0.71 on the Q^{3a} surface.

Partial number density profiles normal to the surface, divided into contributions from the lipid head, lipid tail, and water phase, are shown in Fig. 3. For the purposes of this plot, all hydrogen atoms in the system are excluded from the number density. Additionally, we define the lipid head atoms to include not only atoms in the choline, phosphate, and glycerol moieties but also atoms in the carboxyl group of the palmitic acid tails. The lipid tail atoms encompass all the remaining carbon atoms in the lipid molecule. The separation between the bilayer and surface, measured from the mean position of the head group atoms (as defined above) in the leaflet adjacent to the surface, decreases from Q^4 to Q^2 to Q^3 to Q^{3a}. The Q^4 surface has a fully developed surface water layer and the thickness of the bilayer (measured between the mean head group positions in each leaflet) is significantly less than those on the other surfaces. In fact, the profile across the leaflet adjacent to the surface is very similar to that of the free leaflet at the bulk water interface. Unsurprisingly, the intervening water is more ordered on the crystalline surfaces than the amorphous surface.

The publication by Vishnyakov *et al.*[26] details a study of the separation between a fully periodic DMPC bilayer and an amorphous silica surface as a function of the disjoining pressure, which was imposed by a constant gravity type field applied to all atoms in the bilayer while the substrate was anchored in position. Pores in the substrate allowed the intervening water to equilibrate with the bulk reservoir. The disadvantage of their system is that the periodic nature of the bilayer ensures that surface density is essentially fixed. Our results, however, show that the area per lipid in the adhering bilayer increases significantly. They identify two stable states: α-films with an equilibrium separation of 0.37 nm and β-films with an equilibrium separation of 2.6 nm. In this study, spontaneous α-film formation was observed, suggesting that the thermal energy available at biological temperatures is sufficient to overcome the free energy barrier separating the β-state from the α-state.

There are no hydrogen bonds between the silica and bilayer on the Q^4 surface since there are no donors in either phase. On the Q^2 surface, the relatively large separation of 0.72 nm between the bilayer and surface probably contributes to the small number of hydrogen bonds formed. Less than 1% of the silanols on the surface form hydrogen

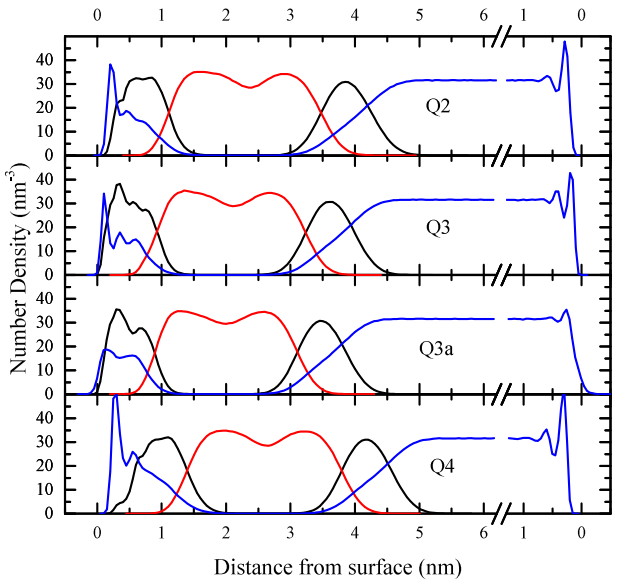

FIG. 3. Number density profiles across the central section of the adsorbed bilayer. The origin on the abscissa corresponds to the average position of the superficial silica oxygen atoms. The right-hand side shows density profiles near the non-adsorbing surface. Black: Lipid head group atoms. Red: Lipid tail group atoms. Blue: Water molecules.

bonds with lipid molecules at any given time. The presence of the bilayer has some effect on the hydrogen bonding between the silanols and water molecules: the fraction of silanols accepting hydrogens from water is around 24%, compared to 30% in the absence of the bilayer, while the fraction acting as a donor actually increases slightly from 27% to 28%.

The Q^2 and Q^4 surfaces account for the two weakest bilayer adhesion strengths. On both the amorphous and crystalline Q^3 surfaces, the separation is only around 0.5 nm, and here there are a significant number of hydrogen bonds forming. In all of these hydrogen bonds, the oxygen sites bonded to phosphorus act as receptors. This suggests that the presence of silica-lipid hydrogen bonds increases the adhesion strength, yet cannot account for the much stronger adhesion on the Q^{3a} surface in comparison to Q^3. In fact, the density of such hydrogen bonds is slightly greater on the Q^3 surface, where 20% ± 3% of the silanols form hydrogen bonds with lipids compared to 15% ± 2% of silanols on the Q^{3a} surface. On both these surfaces, a moderate decrease in the fraction of silanols donating hydrogen atoms to hydrogen bonds with water was observed, from 85% ± 5% to 71% ± 3% on the Q^3 surface and from 62% ± 4% to 53% ± 2% on the Q^{3a} surface. The decrease in the fraction of silanols acting as acceptor in hydrogen bonds with water was more marked on the Q^3 surface, falling from 74% ± 7% to 24% ± 1% in the presence of the bilayer. On the Q^{3a} surface, this effect was less pronounced, producing a decrease from 50% ± 5% to 21% ± 1%.

One obvious difference between the amorphous and crystalline surface is the lack of structure in the fluid phases on the Q^{3a} surface as evidenced by the density profiles in Fig. 3. One consequence is that there is significant overlap between the water-water hydrogen bond profile and silica-water hydrogen bond profile shown in the supplementary material. This facilitates greater networking of hydrogen bonds on the Q^{3a} surface.

Included in Table II are values for the bilayer adhesion enthalpy per unit area on each surface. These values were estimated from simulations containing a fully periodic bilayer and four surface units (approximately 6×6 nm). The number of lipids in the bilayer was chosen such that the lipid surface density matches as closely as possible area per lipid of adsorbed bilayer as recorded in Table II. In the first simulation, the bilayer was situated at the surface, with the number of water molecules between the bilayer and surface also matching the adsorbed density profile. The second simulation contained equal numbers of lipid and water molecules but in this case the bilayer was situated in the middle of water phase. The adhesion enthalpy per unit area was then determined by the difference in total enthalpy between the two simulations.

On all surfaces, barring the Q^2 surface, the enthalpy per unit area was negative and of greater magnitude than the adhesion strength, indicating that the entropic contribution to the free energy opposes adhesion. This is to be expected considering the reduced mobility of the SLB opposed to the free bilayer. Similar results were observed for adhesion on gold surfaces.[21] The entropic contribution opposing adhesion on the Q^{3a} surface appears particularly large, perhaps reflecting greater reduction in lipid mobility on the rougher amorphous surface. The exception is the Q^2 surface where the measured enthalpy was positive. This suggestion that adhesion on this surface was driven by an increase in entropy reflects our observation in Sec. III B that single lipid adsorption was also entropically driven.

In an attempt to identify the source of the increase in disorder, we monitored the orientations of the silanol OH bonds in the plane of the surface during the simulation. The degree of disorder was gauged by the mean resultant length,[33] r, of the angle each bond forms with the y axis, measured on each surface in each configuration of the simulation trajectory. Note that when r is zero the angles are uniformly dispersed and the variation in the direction of the bond vanishes as r approaches one, indicating a highly ordered alignment. In the absence of the bilayer, the time averaged value was 0.742 and decreases to 0.713 when the bilayer is adhering to the surface, with uncertainties less than 0.001. This is the likely source of the increase in disorder driving adhesion and adsorption on the Q^2 surface.

IV. CONCLUSIONS

This paper details the study of four model silica surfaces: (1) a fully hydroxylated crystalline α-quartz (100) surface (Q^2) featuring geminal silanols, (2) a fully hydroxylated crystalline α-cristobalite ($10\bar{1}$) surface (Q^3) featuring isolated silanols, (3) a fully hydroxylated amorphous α-cristobalite ($10\bar{1}$) surface (Q^{3a}) featuring a mixture of isolated and vicinal silanols, and (4) a fully dehydroxylated amorphous α-cristobalite ($10\bar{1}$) surface (Q^4) without silanols.

The immersion enthalpy varied linearly with the surface density of hydrogen bonds formed between the silica and water. In general, silanols involved in mutual interaction hydrogen bond with a neighbouring silanol were less likely to form hydrogen bonds with water molecules. Most of the silanols on the Q^2 surface (96%) were involved in mutual interaction. By contrast, 96% of the silanols on the Q^3 surface and 63% of the silanols on the Q^{3a} surface were not involved in mutual interactions. Hence the surfaces rank in order of increasing hydrophilicity by Q^4, Q^2, Q^{3a}, and Q^3 despite the Q^2 surface having the greatest silanol surface density.

Single lipid adsorption was strongest on the Q^4 surface due to hydrophobic interactions between the lipid carbon tails and the bridging oxygen sites on the surface. The lipid also adsorbs onto the Q^{3a} surface but only weakly on the Q^2 and Q^3 surfaces. The entropic contribution opposes adsorption on all surfaces except the Q^2 surface.

On the crystalline surfaces, the adhesion strength, k_w, is well described by a linear function of the silanol-bilayer hydrogen bond surface density with each hydrogen bond contributing an additional -0.51×10^{-21} J to the adhesion strength compared to the Q^4 surface. Around 20% of the isolated silanols on the Q^3 surface form hydrogen bonds with the lipid bilayer but less than 1% of the mutually interacting silanols on the Q^2 surface. However, the adhesion strength on the Q^{3a} surface does not obey the linear dependence on hydrogen bond

density and is 2.4 times stronger at −2.7 mN m^{-1} than it would be if it behaved like the crystalline surfaces, where a silica-bilayer hydrogen bond density of 0.81 nm^{-2} would give an adhesion strength of −1.13 mN m^{-1}.

On the Q^{3a} surface, 15% of the silanols were donors in hydrogen bonds with lipid molecules. Of these donating silanols, 90% were not involved in mutual interactions. This, together with the negligible incidence of silanol-lipid hydrogen bonding on the Q^2 surface, offers support to the notion that silanols involved in mutual interactions are not available for hydrogen bonding with lipid molecules. The relatively strong adhesion on the Q^{3a} surface raises the possibility that the energy associated with silanol-lipid hydrogen bonds on this surface is of greater magnitude than on the crystalline surfaces. To test this hypothesis quantitatively would require *ab initio* simulation; however, it is interesting to note the relatively large proportion of silanols on this surface that were involved in multiple silanol-water hydrogen bonds, suggestive that the surface morphology favours hydrogen bonding on certain silanols.

With respect to nanoparticle translocation, our value for the adhesion strength for Q^{3a} of −2.7 mN m^{-1} implies a critical diameter from elastic theory of 16 nm for lipid bilayer adhesion of amorphous nanoparticles which is consistent with the experimental work of Pera *et al.*[18] on similar but not identical materials. In particular, the silica nanoparticles (Ludox LS) used by Pera *et al.*[18] are formulated with pH > 7 so that some silanol groups are de-protonated, creating a negative charge on the particle surfaces as well as counter ions in solution, and the vesicles contained DOPC lipids, not DMPC. The behaviour of our fully protonated model silica surfaces for DMPC indicates that *crystalline* silica nanoparticles are unlikely to bind to bilayer membranes for diameters <30 nm; however, very small *amorphous* nanoparticles may do so. The variation of adhesion energy with pH will be the subject of future work.

These results lend credence to recent work[20] on the nature of silica particle toxicology suggesting that membranolysis is not related to silanol density but to silanol disorganisation. In particular, increased membranoltytic activity is proposed to occur when the surface is heterogeneous, comprising both interacting isolated silanols and non-interacting isolated silanols. Our results show that when the surface (and by extension the silanols) is the most disordered, the adhesion strength of the surface for surfactant membranes is the strongest and likely therefore to cause the most disruption to the pulmonary surfactant in alveolar spaces as well as maximising the chances of translocation through epithelial membranes, via lipid envelopment. Note that this finding is equally likely to apply to ostensibly crystalline materials which in nature may present a superficial amorphous layer (Beilby layer), for example, when the crystals have been fractured.

SUPPLEMENTARY MATERIAL

See supplementary material for charge and hydrogen bond density profiles for silica-water and silica-bilayer interfaces and data on preferential binding sites for single lipid adsorption.

ACKNOWLEDGMENTS

We acknowledge funding from the European Union's Horizon 2020 research and innovation programme under Grant Agreement No. 686098, "Smartnanotox" and access to supercomputing facilities though the ARCHER UK National Supercomputing Service.

[1] C. Buzea, I. I. Pacheco, and K. Robbie, "Nanomaterials and nanoparticles: Sources and toxicity," Biointerphases **2**(4), MR17–MR71 (2007).
[2] M. Kendall and I. Lynch, "Long-term monitoring for nanomedicine implants and drugs," Nat. Nanotechnol. **11**, 206–210 (2016).
[3] B. Scharf, C. C. Clement, V. Zolla, G. Perino, B. Yan, S. G. Elci, E. Purdue, S. Goldring, F. Macaluso, N. Cobelli, R. W. Vachet, and L. Santambrogio, "Molecular analysis of chromium and cobalt-related toxicity," Sci. Rep. **4**(1), 5729 (2015).
[4] W. H. De Jong and P. J. Borm, "Drug delivery and nanoparticles: Applications and hazards," Int. J. Nanomed. **3**, 133–149 (2008).
[5] See http://www.smartnanotox.eu/ for an example of the considerable investment made by the EU in nanosafety research in the H2020 programme, via the EU NanoSafety Cluster and in particular the SmartNanoTox project.
[6] K. Kettler, K. Veltman, D. van de Meent, A. van Wezel, and A. J. Hendriks, "Cellular uptake of nanoparticles as determined by particle properties, experimental conditions, and cell type," Environ. Toxicol. Chem. **33**, 481–492 (2014).
[7] R. Michel, E. Kesselman, T. Plostica, D. Danino, and M. Gradzielski, "Internalization of silica nanoparticles into fluid Liposomes: Formation of interesting hybrid colloids," Angew. Chem., Int. Ed. **53**, 12441–12445 (2014).
[8] Y. Roiter, M. Ornatska, A. R. Rammohan, J. Balakrishnan, D. R. Heine, and S. Minko, "Interaction of nanoparticles with lipid membrane," Nano Lett. **8**, 941–944 (2008).
[9] W. Helfrich, "Elastic properties of lipid bilayers: Theory and possible experiments," Z. Naturforsch. C **28**(11), 693 (1973).
[10] M. Deserno and W. M. Gelbart, "Adhesion and wrapping in colloid–vesicle complexes," J. Phys. Chem. B **106**(21), 5543–5552 (2002).
[11] M. Deserno, "Elastic deformation of a fluid membrane upon colloid binding," Phys. Rev. E **69**, 031903 (2004).
[12] D. B. Warheit, T. R. Webb, V. L. Colvin, K. L. Reed, and C. M. Sayes, "Pulmonary bioassay studies with nanoscale and fine-quartz particles in rats: Toxicity is not dependent upon particle size but on surface characteristics," Toxicol. Sci. **95**(1), 270–280 (2006).
[13] S. Takenaka, W. Moller, M. Semmler-Behnke, E. Karg, A. Wenk, O. Schmid *et al.*, "Efficient internalization and intracellular translocation of inhaled gold nanoparticles in rat alveolar macrophages," Nanomedicine **7**(6), 855–865 (2012).
[14] C. Contini, M. Schneemilch, S. Gaisford, and N. Quirke, "Nanoparticle–membrane interactions," J. Exp. Nanosci. **13**(1), 62–81 (2018).
[15] T. H. Anderson, Y. Min, K. L. Weirich, H. Zeng, D. Fygenson, and J. N. Israelachvili, "Formation of supported bilayers on silica substrates," Langmuir **25**(12), 6997–7005 (2009).
[16] M. C. Watson, E. G. Brandt, P. M. Welch, and F. L. H. Brown, "Determining biomembrane bending rigidities from simulations of modest size," Phys. Rev. Lett. **109**(2), 028102 (2012).
[17] F. G. Strobl, F. Seitz, C. Westerhausen, A. Reller, A. A. Torrano, C. Bräuchle, A. Wixforth, and M. F. Schneider, "Intake of silica nanoparticles by giant lipid vesicles: Influence of particle size and thermodynamic membrane state," Beilstein J. Nanotechnol. **5**, 2468–2478 (2014).
[18] H. Pera, J. M. Kleijn, and F. A. M. Leermakers, "Interaction of silica nanoparticles with phospholipid membranes," Chem. Lett. **41**(10), 1322–1324 (2012).
[19] C. Pavan, M. Tomatis, M. Ghiazza, V. Rabolli, V. Bolis, D. Lison, and B. Fubini, "In Search of the chemical basis of the hemolytic potential of silicas," Chem. Res. Toxicol. **26**(8), 1188–1198 (2013).
[20] C. Pavan and B. Fubini, "Unveiling the variability of "quartz hazard" in light of recent toxicological findings," Chem. Res. Toxicol. **30**(1), 469–485 (2017).
[21] M. Schneemilch and N. Quirke, "Free energy of adsorption of supported lipid bilayers from molecular dynamics simulation," Chem. Phys. Lett. **664**, 199–204 (2016).
[22] J. P. M. Jämbeck and A. P. Lyubartsev, "Derivation and systematic validation of a refined all-atom force field for phosphatidylcholine lipids," J. Phys. Chem. B **116**(10), 3164–3179 (2012).

[23]J. P. M. Jämbeck and A. P. Lyubartsev, "An extension and further validation of an all-atomistic force field for biological membranes," J. Chem. Theory Comput. **8**(8), 2938–2948 (2012).
[24]J. P. M. Jämbeck and A. P. Lyubartsev, "Another piece of the membrane puzzle: Extending slipids further," J. Chem. Theory Comput. **9**(1), 774–784 (2013).
[25]F. S. Emami, V. Puddu, R. J. Berry, V. Varshney, S. V. Patwardhan, C. C. Perry, and H. Heinz, "Force field and a surface model database for silica to simulate interfacial properties in atomic resolution," Chem. Mater. **26**(8), 2647–2658 (2014).
[26]A. Vishnyakov, T. Li, and A. V. Neimark, "Adhesion of phospholipid bilayers to hydroxylated silica: Existence of nanometer-thick water interlayers," Langmuir **33**(45), 13148 (2017).
[27]Y. Li, M. Liao, and J. Zhou, "Catechol–cation adhesion on silica surfaces: Molecular dynamics simulations," Phys. Chem. Chem. Phys. **19**(43), 29222–29231 (2017).
[28]S. H. Lee, R. J. Stewart, H. Park, S. Goyal, V. Botu, and H. Kim *et al.*, "Effect of nanoscale roughness on adhesion between glassy silica and polyimides: A molecular dynamics study," J. Phys. Chem. C **121**(44), 24648–24656 (2017).
[29]W. Stöber, A. Fink, and E. Bohn, "Controlled growth of monodisperse silica spheres in the micron size range," J. Colloid Interface Sci. **26**(1), 62–69 (1968).
[30]J. S. Hub, B. L. de Groot, and D. van der Spoel, "g_wham—A free weighted histogram analysis implementation including robust error and autocorrelation estimates," J. Chem. Theory Comput. **6**(12), 3713–3720 (2010).
[31]T. Takei and M. Chikazawa, "Origin of differences in heats of immersion of silicas in water," J. Colloid Interface Sci. **208**(2), 570–574 (1998).
[32]O. Saengsawang, T. Remsungnen, S. Fritzsche, R. Haberlandt, and S. Hannongbua, "Structure and energetics of water–Silanol binding on the surface of silicalite-1: Quantum chemical calculations," J. Phys. Chem. B **109**(12), 5684–5690 (2005).
[33]K. Mardia, *Statistics of Directional Data* (Academic Press, New York, 1972).